Muzzle Brake Optimization

Allen Dominek

Abstract

CFD numerical simulations of muzzle brakes were performed to improve and optimize its recoil performance. The base design chosen had significant baffle area which is an important feature since it is the gas pressure within the port acting on the surface area to produce the force which minimizes the recoil force. The controlling geometric feature which limits the forward force was identified and removed resulting in significant improvement. The optimized design was fabricated and tested to validate the design.

Keywords: muzzle brake, recoil, CFD, optimization

1. Introduction

There are many muzzle brakes available to reduce recoil along with many articles and videos comparing their effectiveness. The basic principle in their design is to have the gas generated from the powder burn to impact the muzzle brake baffles. The high pressure gas impinging against the baffles creates a force driving the rifle forward. The generated force is dependent upon the pressure of the gas and the effective area of the baffle the gas is impressed upon.

A numerical study was conducted to analyze the performance of muzzle brakes using computational fluid dynamics (CFD). This analysis indicated how the geometry of the muzzle break could be changed to significantly improve its performance. An optimized design was then fabricated and tested.

2. Reference Designs

Muzzle brakes typically have a cylindrical shape most likely due to ease of manufacture and cost. The number of ports varies for a muzzle brake but it is dependent upon the powder charge and bullet caliber for the firearm. Recoil measurements were made using four reference designs.

Figure 1 illustrates four muzzle brakes used in this testing. Two have a rectangular cross-section and two have a cylindrical cross-section. The rectangular shaped muzzle brakes were made by the author. The cross-sectional shape was essentially 1″x2″. MB1 was based upon a muzzle brake provided by [1]. MB3 was obtained from [2]. MB2 had essentially the same cross-section shape as MB1 but with the port dimensions of those in MB3. MB4 was obtained from an eBay site. The essential dimensional data for these muzzle brakes are provided in Table 1.

Figure 1: Illustration of the four, 3 ported muzzle brakes used.

Table 1

Muzzle brake parameters (inches)

Parameter	Port width	Port height	Port depth	Bore diameter
MB1	.596	.800	1.880	.319
MB2	.325	.775	1.980	.312
MB3	.340	.550	.826	.372
MB4	.390	.665	.980	.340

3. CFD Modeling

The use of CFD for muzzle brake analysis is not new. There are many past works as indicated in [3, 4, 5, 6, 7, 8, 9, 10, 11, 12]. In this study, the impact of the muzzle brake was calculated for muzzle brake MB1 using OpenFOAM [13] and integrating the HiSA solver [14] with it. The numerical modeling is discussed more in detail at [15]. The numerical model employed a quarter sphere for the calculation domain as shown in Figure 2. It used three different mesh densities for a total of 1,269,378 cells. The mesh was generated by cfMESH from the CfdOF workbench of FreeCAD [16]. The workbench also generated the initial input files for the OpenFOAM simulation but these were edited for use with the HiSA solver.

The mesh had 5 boundary surfaces with each having a unique boundary condition. The boundary condition on the spherical surface was set to a far-field condition, the two planar surfaces were set to a symmetry condition, the metal surfaces were set to a no-slip condition and the surface representing the muzzle opening of the barrel was set to an inlet condition. The inlet

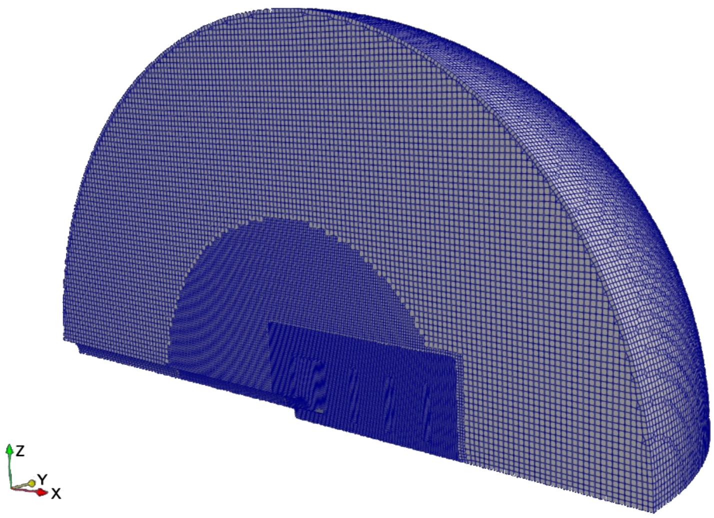

Figure 2: The meshed calculation domain for the CFD simulation.

boundary conditions are described later. Figure 3 illustrates the geometry and the location of the inlet/muzzle surface shown in red.

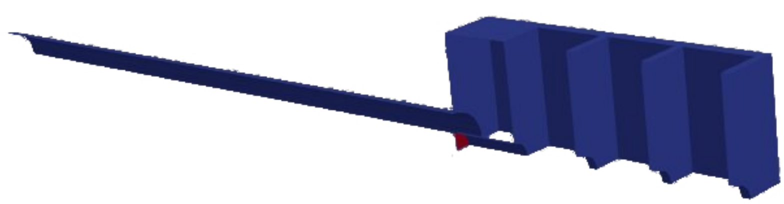

Figure 3: Illustration of the geometry and location of the inlet surface (shown in red).

[Temporarily excerpted]

4. Optimization Process

[Temporarily excerpted]

5. Recoil Measurements

Recoil measurements have been done for a long time using a variety of techniques [15, 17, 18, 19] as examples. Mounting firearm receivers on sleds to measure recoil forces has also been done. One novel approach has been to orient the sled on an angle as shown in Figure 4 [20]. The amount of kinetic energy can then be determined by measuring the displacement height for a fired round since by the conservation of energy, the transfer of kinetic energy to potential energy will be equal. It should be noted that only $\cos(20) * KE$ will equal the potential energy for the way the firearm is mounted to the fixture. Note that linear ball bearing blocks have friction and limited acceleration rates so the true kinetic energy cannot be determined using this approach but relative recoil forces can.

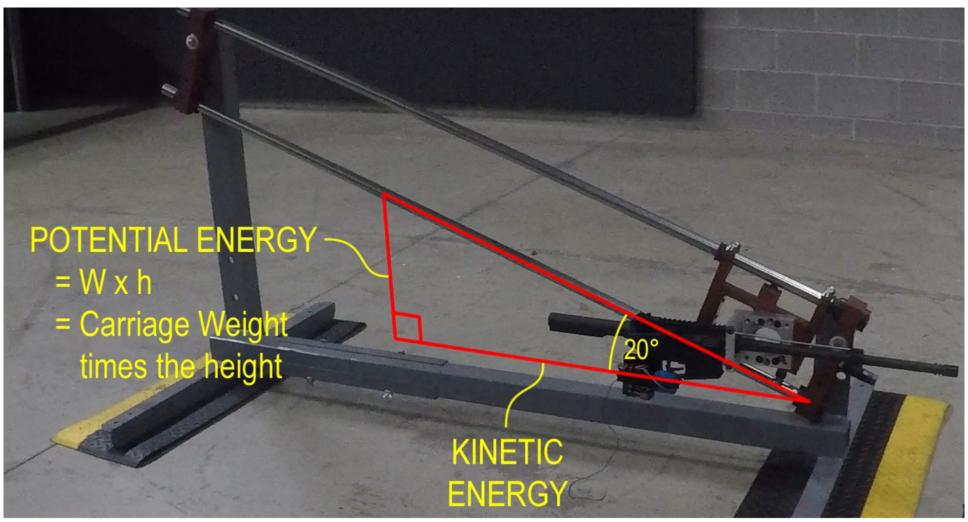

Figure 4: Illustrating the use of a slanted rail system to measure the kinetic energy of a recoil [20]. Note that the potential energy is actually W*h*g where g is the gravitational constant.

The slant angle, θ, has an impact on the measurement resolution available. The distance that the sled moves along the rods is equal to $d = h_{max}/\sin(\theta)$. The greater d is, the greater the resolution is. The highest resolution is when the rods are horizontal but that would require very long rods unless there is sufficient drag in the sled fixture.

The equation of motion for this system is

$$F = mx'' = -F_g - F_d \tag{1}$$

where m is the system mass, x is the position along the rail, x'' is the second derivative with respect to time, $F_g = mg$ is the restoring force of gravity, g, and F_d is the resistive drag force of the system. Integrating twice yields the solution to this system as

$$x(t) = .5(g + F_d/m)t^2 + at + b \tag{2}$$

The excitation of the system caused by the firing of the firearm is extremely short ($\approx$ 1 ms) compared to the response time of the system. This lends itself to the use of the initial conditions $x(0) = 0$ and $x'(0) = v_0$ to determine the coefficients, a and b. v_0 is the velocity of the firearm in the horizontal direction. The coefficients are:

$$a = v_0 \cos(\theta),$$
$$b = 0$$

and the parameter maximums are:

$$t_{max} = v_0 \cos(\theta)/(g + F_d/m),$$
$$x_{max} = .5 * v_0^2 \cos^2(\theta)/(g + F_d/m),$$
$$h_{max} = x_{max} \sin(\theta) = .5 * v_0^2 \cos^2(\theta) \sin(\theta)/(g + F_d/m).$$

For a $v_0 = 7$ ft/s, $F_d = 0$ and $\theta = 20$ degrees, $t_{max} = .2$ s, $x_{max} = 8.6''$ and $h_{max} = 2.7''$. F_d is the force required to move the system (firearm mounted to the rails). This can be measured with a simple force scale attached the rails' carriage pulling parallel to the rails.

A downside to this fixture, as shown, is that when the sled returns to the initial position, it is traveling at several ft/s and abruptly lands into the base.

Gravity can be used in other configurations to impede the recoil during measurements. One configuration is to vertically position the rails with the firearm pointing vertically downward with a bullet catcher on the floor. This is much more compact and provides the full firearm velocity. For a $v_0 = 7$ ft/s, the displacement is 9.1 inches. This configuration offers more resolution since the displacement is greater than the slanted configuration at 20 degrees.

In this study, a horizontal rail system was used to measure the recoil for a muzzle without and with the reference muzzle breaks. The kinetic energy generated in this configuration was absorbed using a spring as shown in Figure 5. An o-ring on one of the rails was used to mark the maximum extent of the carriage displacement. The spring was acquired through McMaster Carr with the part number of 5108N647.

The equation for motion when a spring is used as a restoring force is

$$F = mx'' = -F_s - F_d \tag{3}$$

where m is the system mass, x is the position along the rail, x'' is the second derivative with respect to time, $F_s = a_s x + b_s$ is the restoring force of the spring, and F_d is the resistive drag force of the system. The ODE then is

$$x''(t) + a_s/mx = -(b_s + F_d)/m. \tag{4}$$

The solution to this system is

$$x(t) = a\cos(\omega t) + b\sin(\omega t) + x_p \tag{5}$$

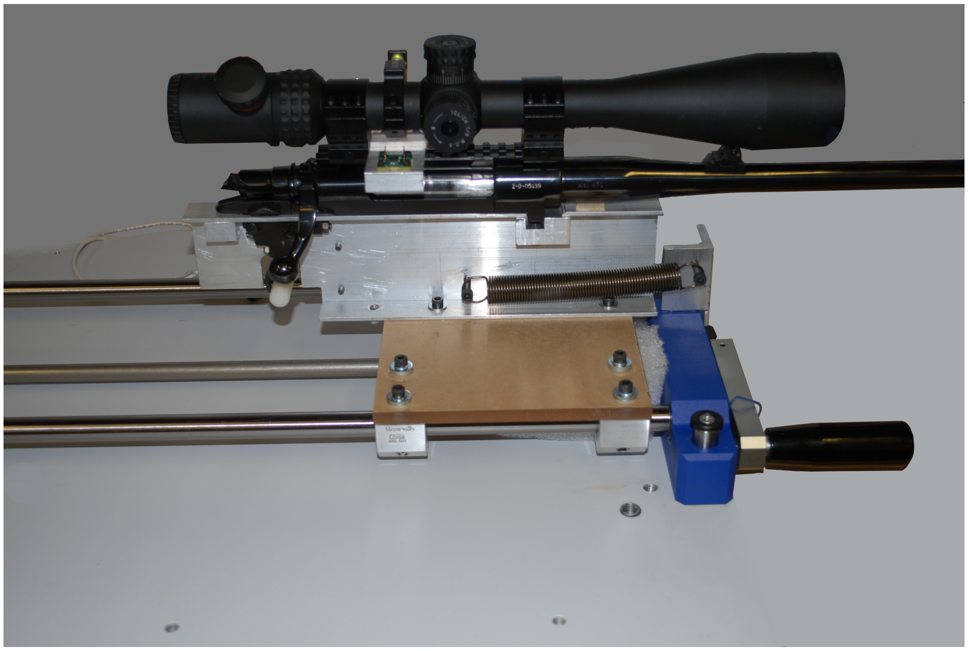

Figure 5: Fixture for spring stretching force measurement.

where $\omega = \sqrt{(}a_s/m)$ is the natural oscillation frequency.

Solving for x_p (the particular solution being a constant) yields

$$
\begin{aligned}
0 + a_s/mx_p &= -(b_s + F_d)/m \\
x_p &= -(b_s + F_d)/a_s
\end{aligned}
$$

The constants a and b can be determined with the initial conditions $x(t) = 0$ and $x'(0) = v_0$. The first condition defines a to be

$$a = -(b_s + F_d)/a_s \tag{6}$$

and using

$$x'(t) = -a\omega \sin(\omega t) + b\omega \cos(\omega t) \tag{7}$$

with the second condition defines b to be

$$b = v_0/\omega. \tag{8}$$

The maximum spring displacement and time occurs when $v = x'(t_{max}) = 0$. These values are given by

$$
\begin{aligned}
t_{max} &= atan(c2/c1)/\omega \\
x_{max} &= c1 \cos(\omega t_{max} + c2 \sin(\omega t_{max}) - (b_s + F_d)/a_s \\
&\text{or} \\
x_{max} &= \sqrt{(}c1^2 + c2^2) - c1
\end{aligned}
$$

Temporarily
Excerpted

Figure 6: Illustration of muzzle brake MB6_6.

Note that a spring is not the only way to generate a force to resist or restore the system. One could induce greater drag into the rail system by having a frictional clamp mounted to the rail as long as it was consistent between shots. This would eliminate the abrupt stopping the other configurations experience. Alternatively, one could suspend a weight using a pulley and a cable to provide another form of drag that would be constant.

6. Measurement Verification

In these measurements, the powder used was IMR 4350 with a load charge of 43.7 grains. The bullet used was a 162 grain Hornady ELD-Match bullet in a Remington 7-08 case. The measured muzzle velocity is 2550 ft/s for the configuration as measured with a chronograph. Three rounds were fired for each configuration. Figure 6 illustrates the MB6_6 muzzle brake.

Figure 7 illustrates the amount the spring stretched for each configuration. Figure 8 illustrates the maximum force experience for each configuration. Clearly, the MB_6 muzzle brake is superior in performance.

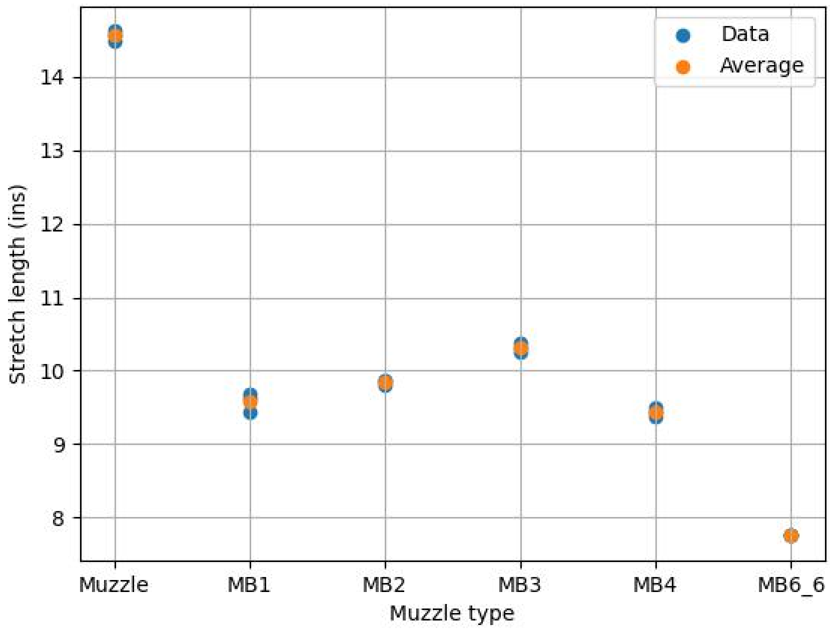

Figure 7: The measured stretched spring lengths for the various configurations.

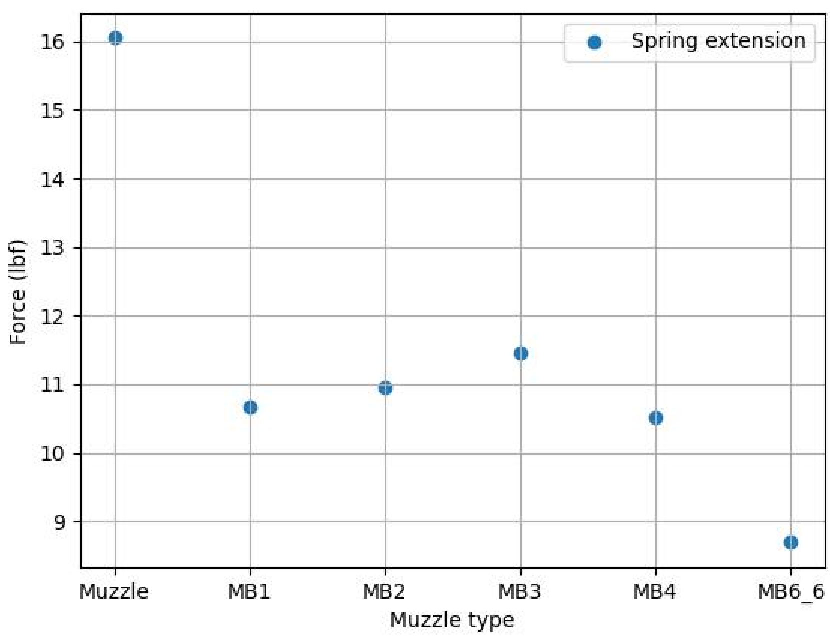

Figure 8: The measured maximum force generated for the various configurations when constrained by a spring.

The resulting velocity of the firearm with each muzzle break can now be deduced with the data shown in Figure 7 using the equation of motion. Using the measured data shown in Table 2, the spring's force vs displacement equation is

Table 2

Measured spring displacement

Displacement (in)	Force (lbs)
1.75	2.5
4.25	5
9	10
13.625	15

$$F_s = .3106 + 1.081x \tag{9}$$

with x in inches and F_s in lbs. This makes $a_s = 1.081$ and $b_s = .3106$. Note that with this linear regression, the force is not equal to zero when the displacement is equal to zero. This is because the spring is non-linear and is stiffer with small displacements than with larger displacements. This is not a concern since the displacements of interest are larger where the linear regression is accurate.

Table 3 contains the processed data for the muzzle measurements. The initial velocity, v_0 is shown for each measurement. These velocity values were found numerically by using the motion equation, Eq. 5. The velocities listed in Table 3 generate the spring displacement using the motion equation. Figure 9 illustrates the efficiency based upon the measured displacement and inferred v_0 values. The efficiency equations used are

$$\begin{aligned} \text{eff}_{dis} &= (1. - \text{dis}_i/\text{dis}_{muz}) * 100 \\ \text{eff}_{vel} &= (1. - v_{0i}/v_{0muz}) * 100 \end{aligned}$$

where muz refers to the no muzzle brake case. There is a minor difference between the two efficiency definitions. The offset is due to errors in the measurement/model.

As shown in Table 3, the effect of a muzzle brake is to reduce the recoil velocity. For the MB1 and MB6_6, the velocity reduction is 2.77 and 3.83 ft/s, respectively. Numerically, the velocity reduction can be calculated from the force calculations shown in Figure [temporarily excerpted]. This is accomplished by calculating the moment (integrating the force over time) and dividing the system's mass (firearm and mounting components to the rails). The CFD calculated velocity reductions for MB1 and MB6_6 is 2.95 and 4.09 ft/s, respectively. Table 4 compares the measured and calculated velocity reductions for these two muzzle brakes. The variations between the

Table 3

Firearm Results

Muzzle Brake	Displacement (in)	Force (lbs)	Velocity (ft/s)
None	14.56	16.05	7.91
MB1	9.58	10.67	5.14
MB2	9.85	10.96	5.27
MB3	10.31	11.45	5.58
MB4	9.44	10.51	5.13
MB6_6	7.75	8.68	4.08

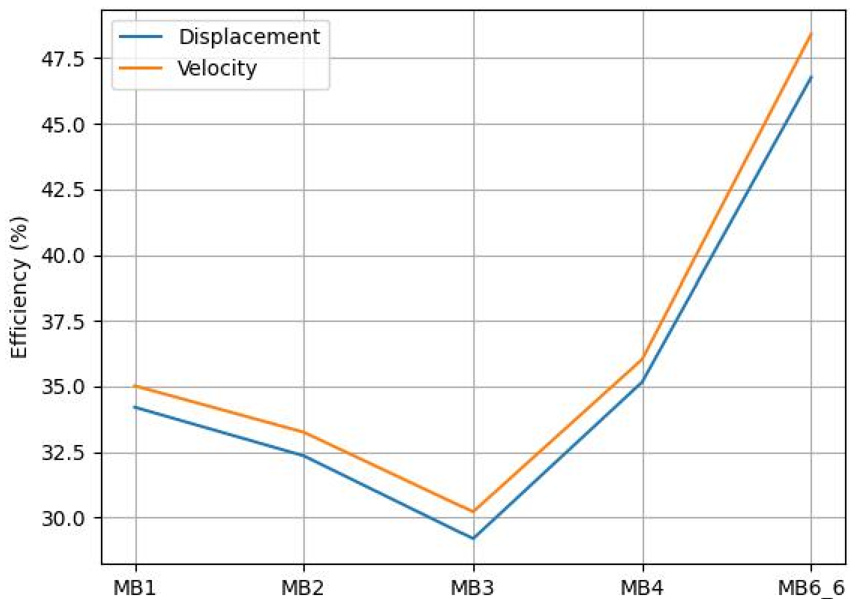

Figure 9: Muzzle brake efficiencies using displacement and velocity data.

measured and calculated quantities is roughly 6%, a reasonable level of variation considering measurement and model error.

Table 4

Muzzle Reduction Velocities

Muzzle Brake	Measured Reductions (ft/s)	Calculated Reductions (ft/s)
MB1	2.77	2.95
MB6_6	3.83	4.09

7. Conclusion

A design change on a muzzle brake was made to significantly improve its performance in reducing recoil. [Temporarily excerpted] The improved muzzle brake design was then fabricated and tested. The measurement confirmed the calculated performance improvement.

References

[1] 4AW, https://4aw-store.myshopify.com/collections/muzzle-brakes/products/4aw-muzzle-brake-3-port.

[2] Silencer Co., https://silencerco.com/shop/asr-muzzle-brake/.

[3] Lei, H., Wang, Z. and Zhao, J., "Stress Analysis of Muzzle Brake by Using Fluid-Solid Coupling Method", *Journal of Engineering Science and Technology Review*, Sept. 4, 2016, pp. 48-55.

[4] Hristov, N. Kari, A. Jerković and Savić S., "Application of a CFD Model in Determination of the Muzzle Blase Overpressure in Small Arms and Its Validation by Measurement", *Tehnicki Vjesnik*, Vol. 15 May 2018, pp. 1399-1407, pp. 36-44.

[5] Chaturvedi E. and Dwivedi, R.K., "Computer aided design and analysis of a tunable muzzle brake", *Defence Technology*, Elsevier, Jun 18, 2018, pp. 89-94.

[6] Fureby, C. and Troeng, C., "A Computational Study of Unsteady Gun Tube Flows", FOI-R–3663–SE, Mar. 2013.

[7] Trebiński, R. and Czyżewska, M., "Estimation of the Increase in Projectile Velocity in the Intermediate Ballistics Period", *Central European Journal of Energetic Materials*, 2015, pp. 63-76.

[8] Zhao, X. and Lu, Y., "S Comprehensive Performance Evaluation Method Targeting Efficiency and Noise for Muzzle Brakes Based on Numerical Simulation", *Energies*, Vol. 15, May 22, 2022, 3576.

[9] Ahmed, N.Z., Jerković, D.D., Hristov, N.P. and Abaci, W.B., "Analytical and Experimental Investigation of the Muzzle Brake Efficiency", Facta Universitatis, Series: Mechanical Engineering, [S.l.], Jun 2022.

[10] Bougamre, A. and Huilin, L., "Multiphase CFD Simulation of Solid Propellant Combustion in a Small Gun Chamber", *International Journal of Chemical Engineering*, Vol. 0214 Hindawi Publishing Corporation.

[11] Olsson, S., Parmhed, O. and Wikström, N., "Projection 2015 Modeling and Experiments", FOI Swedish Defence Research Agency, FOI-R–4170–SE, Oct. 2015.

[12] Ingvarsson, M., Nordin-Bates, K., Olsson, S., Parmhed, O. and Wikström, N., "Methods for measuring recoil and modeling of internal and transitional ballistics processes", FOI Swedish Defence Research Agency, FOI-R–4461–SE, Nov. 2017.

[13] The OpenFOAM Foundation, https://openfoam.org/.

[14] High Speed Aerodynamic (HiSA) solver, Aeronautic Systems Competency Area of the Council for Scientific and Industrial Research https://hisa.gitlab.io/

[15] Dominek, A., "The Measurement of Recoil Force for Small Caliber Arms", https://ballistics-studies.com/article_recoil.pdf.

[16] FreeCAD, 3D parameteric modeler, https://www.freecad.org/

[17] Hall, M.J., "Measuring felt recoil of sporting arms", *International Journal of Impact Engineering*, Vol. 35, Elsevier, 2008 pp. 540-548.

[18] Canfield-Hershkowitz, B., Foster, T. and Meijer, W., "Rifle and Shotgun Recoil Test System", Senior Project, California Polytechnic State University, Dec. 2013.

[19] Lonzi, F., Martarelli, M. Santolini, C. and Scalise, L., "Measurement of firing impulse forces", *Proceedings of ISMA*, 2014, pp. 2065-2075.

[20] Hiperfire, https://www.youtube.com/watch?v=UgZPvJKURe0.